Icarus **151**, 139–149 (2001)
doi:10.1006/icar.2001.6613, available online at http://www.idealibrary.com on IDEAL®

Spectral Properties of Near-Earth Objects: Palomar and IRTF Results for 48 Objects Including Spacecraft Targets (9969) Braille and (10302) 1989 ML

Richard P. Binzel

Department of Earth, Atmospheric, and Planetary Sciences, Massachusetts Institute of Technology, Cambridge, Massachusetts 02139
E-mail: rpb@mit.edu

Alan W. Harris

Jet Propulsion Laboratory, Pasadena, California 91109

Schelte J. Bus

Department of Earth, Atmospheric, and Planetary Sciences, Massachusetts Institute of Technology, Cambridge, Massachusetts 02139

and

Thomas H. Burbine

Department of Mineral Sciences, National Museum of Natural History, Smithsonian Institution, Washington, DC 20560

Received July 24, 2000; revised February 1, 2001

We present results of visible wavelength spectroscopic measurements for 48 near-Earth objects (NEOs) obtained with the 5-m telescope at Palomar Mountain Observatory during 1998, 1999, and early 2000. The compositional interpretations for 15 of these objects have been enhanced by the addition of near-infrared spectra obtained with the NASA Infrared Telescope Facility. One-third of our sampled objects fall in the Sq and Q classes and resemble ordinary chondrite meteorites. Overall our sample shows a clear transition between S-type and Q-type compositional classes over visible and near-infrared wavelengths. Taken together these results point toward an abundance of near-Earth asteroids capable of providing sources for ordinary chondrite meteorites. Our sampling strategy favors targeting the smallest observable objects and we report results for the 15-m diameter object 1998 BT13, the smallest spectroscopically measured NEO to date. NEOs show a greater spectral diversity than main-belt asteroids, and our small sample includes objects falling in the rare categories of K, L, O, and V classes. The K-class object 1999 JD6 is found to match CV chondrite meteorites. Potential spacecraft targets received top priority for observation, with the ordinary chondrite-like composition of (9969) Braille being reported prior to the Deep Space-1 encounter. The relatively accessible asteroid (10302) 1989 ML displays a neutral spectrum that may be interpreted as a shock-darkened ordinary chondrite.

Key Words: **asteroids, composition; meteorites; surfaces, asteroids.**

INTRODUCTION

One of the most fundamental goals in the study of primitive bodies in the Solar System is to achieve an understanding of the relationships between asteroids, comets, and meteorites. Because asteroids, comets, and the immediate source bodies for meteorites exist within the near-Earth object (NEO) population, a compositional investigation of this population provides the best basis for understanding these relationships. In addition, the NEO population poses a long-term collisional hazard to the Earth as well as the future opportunity for utilization of space resources, thus providing a highly important and practical rationale for its study.

We report the results of our ground-based reconnaissance program of NEOs conducted using the 5-m (200-inch) telescope at Palomar Mountain Observatory from January 1998 through January 2000. Our targets were chosen primarily from the sample of known NEOs that lacked previous spectroscopic measurements and from discoveries made just prior to or during our observing runs. Priority was given to those targets having the greatest H magnitude values, as these objects are presumed to be smallest in size. We reached a limit of H = 26 for 1998 BT13, estimated to have a size in the range of 15–20 m (for albedo 0.25 to 0.15), smaller than the size of the Palomar 200-inch dome where we were observing! (See Fig. 1.) We additionally performed directed measurements of objects identified as

0019-1035/01 $35.00

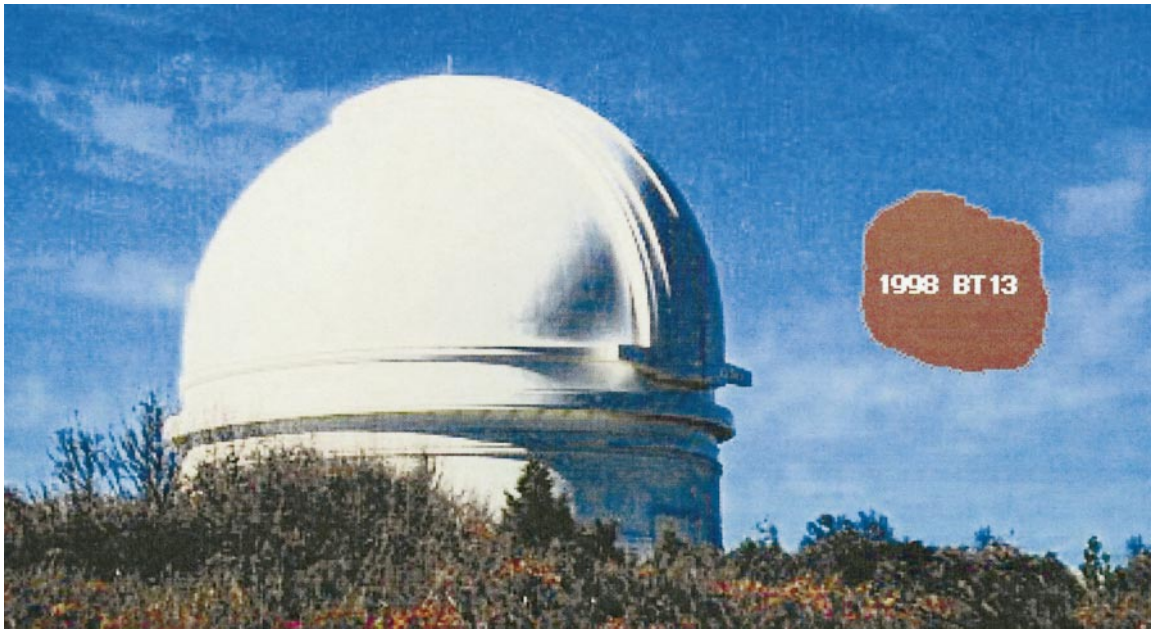

FIG. 1. Schematic diagram for the smallest near-Earth object spectroscopically measured to date, 1998 BT13, which has an estimated size of only 15–20 m. At this size, 1998 BT13 is smaller than the dome of the 200-inch telescope where observations were made.

destinations for spacecraft encounters: (9969) Braille as the target for Deep Space 1 (DS-1) and (10302) 1989 ML as a formerly designated target for MUSES-C. Although not on the target list for any currently approved mission, interest in (10302) 1989 ML remains high because of its relatively easy accessibility from Earth.

PALOMAR INSTRUMENTATION, OBSERVING, AND REDUCTION PROCEDURES

Our Palomar measurements consist of visible wavelength spectra obtained using the Double Spectrograph (Oke and Gunn 1982). This instrument uses a pair of charge–coupled device (CCD) cameras to simultaneously record the blue and red halves of a long-slit spectrum. To increase the signal-to-noise per pixel, and greatly reduce the readout time for our observations, the readout for each 1024 $\times$ 1024 CCD array was binned by a factor of 2 $\times$ 2, and only that fraction of each CCD image containing the spectrum and surrounding sky was stored. Due to different focal lengths for the two CCD cameras, the resulting spatial scales for the blue and red channels are 1.25 and 0.94 arcsec per binned pixel, respectively.

For our observations, separation between the blue and red channels was accomplished using the "D-52" dichroic, which has a steep cutoff in transmission shortward of 0.52 μm. For the blue channel, we utilized the 300 line/mm grating (blazed at 0.399 μm) that gives a dispersion of 7 Å per binned pixel over the usable spectral range of 0.36 to 0.62 μm. For the red channel we utilized the 158 line/mm grating (blazed at 0.75 μm) to give 10 Å per binned pixel dispersion over the range from 0.53 to 0.92 μm, thus providing roughly 0.09 μm of spectral overlap with the blue channel. This overlap is possible since the dichroic does not reach maximum transmission before 0.62 μm. Still, the reflectivity of the dichroic averages less than 10% over the interval of 0.52 to 0.62 μm, so that the usefulness of this overlap region in matching the vertical scaling of the spectral halves is generally limited to the brighter asteroids.

A relatively wide 6-arcsec slit was utilized to maximize the amount of light being sent to the detectors from our faint program objects. The length of the slit was sufficient to provide a region of sky 50 arcsec wide on either side of the object spectrum. This allows for a proper subtraction of the sky during the data reduction. The slit remained fixed in a N–S orientation throughout all observations, and great care was taken to make all observations as close to the meridian as possible, minimizing the effects of differential atmospheric refraction. The capability for the telescope to track at nonsidereal rates in both coordinates allowed for accurately maintaining fast-moving targets in the slit. This tracking was monitored and manually corrected as necessary through the use of a sensitive slit-viewing camera. Under good seeing conditions, the limiting magnitude for measurements extends below V = 19.

Standard data-reduction procedures were followed using packages contained in image reduction and analysis facility (IRAF). Preprocessing of the CCD images involved bias and flat-fielding corrections, using calibration images taken nightly at the telescope. The procedures used to produce the extracted one-dimensional spectra are detailed by Bus (1999) and are essentially the same as described by Xu *et al*. (1995). Upon extraction, each spectrum was rebinned to a uniform dispersion of 25 Å

per pixel. The normalization of these spectra to units of relative reflectance was provided by observations of bright solar analog stars. For this program, we utilized the widely accepted standards Hyades 64 and 16 Cyg B as well as the United Kingdom infrared telescope (UKIRT) standard FS13 and Landolt 102-1081, fainter stars which we found to be comparable in their quality as solar analogs. All objects were reduced in exactly the same manner and as a check, bright main-belt asteroids having previously known spectral characteristics were also occasionally observed. All main-belt results proved consistent with previous measurements. These objects are included within Results.

To accurately merge the blue and red halves of the calibrated spectrum, a third-order polynomial was fit repeatedly over the wavelength range of 0.44 to 0.66 μm and the vertical scaling of the blue half was adjusted with respect to the red half. The best scaling factor was found when the value of chi-squared was minimized for the fitted function. The final combined spectrum was then normalized to unity at 0.55 μm.

IRTF INSTRUMENTATION, OBSERVING, AND REDUCTION PROCEDURES

The visible wavelength measurements obtained at Palomar were complemented by a separate program led by one of us (RPB) that extends the spectral coverage to near-infrared wavelengths through observations using the 3-m NASA Infrared Telescope Facility (IRTF) at Mauna Kea. These IRTF measurements utilized the "asteroid grism" system (designed by Binzel and installed within the facility's NSFCAM infrared camera) that provides coverage over the spectral range of 0.9 to 1.65 μm. The extended spectral coverage provided by the asteroid grism is essential for a more detailed compositional analysis, including comparison with potential meteorite analogs. Despite the inevitable offset in timing between the dates of the Palomar and IRTF runs and the fainter limiting magnitude for most of the Palomar targets, extended spectral coverage was obtained for 15 objects, or roughly one-third of the Palomar sample.

Figure 2 displays the instrument design and details of the "asteroid grism" system consisting of a fused silica grism (a grooved prism) having 75 lines per mm blazed at an angle of 10 degrees and optimized for maximum throughput at 1.319 μm.

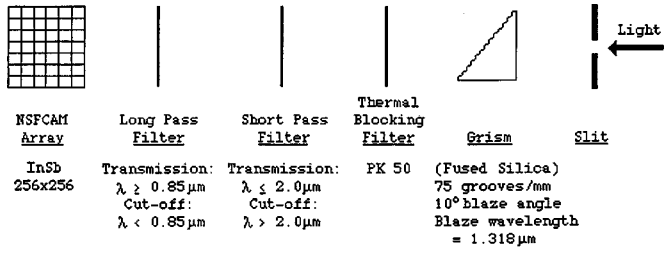

FIG. 2. Component diagram for the NSFCAM "asteroid grism" system utilized at the NASA Infrared Telescope Facility to obtain low-resolution spectra over the range 0.9 to 1.65 μm.

Light first passes through a 1.2-arcsec slit before entering the flat face of the grism. Dispersed light from the grism then passes through a PK50 filter to block the transmission of thermal radiation to the thermally sensitive detector. The grism and the PK50 reside within the CVF wheel of the NSFCAM system. The wavelength range for usable spectra is determined by a pair of blocking filters residing within the NSFCAM filter wheel. This combination consists of a short pass filter that transmits radiation shortward of 2 μm and a long pass filter that transmits radiation longward of 0.85 μm. (All cut-on and cut-off wavelengths are the half-power points for steep regions of the spectral transmission curves.) The resulting light that reaches the NSFCAM 256 $\times$ 256 InSb array covers the range of 0.85 to 2 μm. Only the light from the first-order spectrum, covering approximately 0.85 to 1.65 μm is usable as the second-order spectrum begins contaminating the region 1.7 to 2.0 μm. The resulting spectral resolution of the system is $\lambda/d\lambda \sim 100$, where the first-order spectrum covers $\sim$64 pixels on the NSFCAM CCD with a dispersion of $\sim$0.014 μm/pixel. Wavelength calibration was achieved by imaging a flat lamp through narrow band filters and measuring the pixel locations of the first-and second-order images of the slit. Full details of the setup and operation of the "asteroid grism" are given in the IRTF internal manual *NSFCAM Asteroid Grism: A User's Guide* by R. P. Binzel.

The IRTF observing and reduction procedures follow closely those used for visible wavelength spectroscopy described in the previous section (slit fixed in a north–south orientation, all measurements made near the meridian, similar choices in solar analog stars, etc.). We found a practical limiting magnitude near $V = 18$, where a SNR of $\sim$3 is achieved in 240 s total integration time. Typically one hour or more total integration time was used on each object. For these near-IR measurements, spectral images were always obtained in pairs offset by 10–12 arcsec north–south along the slit. These paired observations (noted as A and B spectra) provided near-simultaneous sky and bias measurements in the same pixels where the spectral measurements were made. A first step in the reduction process was to form bias- and sky-subtracted images A–B and B–A. Any residual sky or bias signal in the image frames was fit and subtracted during the spectral extraction process using IRAF. In all cases, the A spectra were reduced, averaged, and converted to reflectance (through division by the solar analog) separately from the B spectra. A final comparison of the independent A and B spectra served as a check on the quality of the results. All of the final plots represent the average of the A and B spectra, with error bars based on the Poisson statistics of the total counted photons.

The short wavelength ends of the IRTF spectra typically fall in the range of 0.88 μm, providing 0.04 μm overlap between the Palomar and IRTF data. Merging of the visible and near-infrared spectra was accomplished through the same polynomial fitting and chi-squared minimization technique applied to the two spectral channels within the Palomar system (described above). In this case the scaling adjustment was made to the near-IR

spectrum so as to match with the red channel spectrum normalized to unity at 0.55 μm.

RESULTS

All 48 spectra contained in our combined Palomar and IRTF sample of near-Earth objects are summarized in Table I and presented in Appendix A. Our spectral analysis of these objects utilizes the techniques and taxonomic system developed by Bus (1999). The Bus system is a "feature-based" taxonomy that takes advantage of the higher spectral resolution (relative to filter photometry) obtained with CCD spectrographs. A great advantage of this system is the ability to recognize distinct subdivisions within the previously established broad classes such as "C" and

TABLE I
Observational Results for Near-Earth Objects

Number	Name	Provisional desgination	Orbit	Previous type	New type	Slope	PC2′	PC3′	H Magnitude
1863	Antinous	1948 EA	APO	SU	Sq	0.178	−0.179	0.052	15.5
1943	Anteros	1973 EC	AMO	S	L	0.640	−0.016	−0.069	15.8
1981	Midas	1973 EA	APO		V	−0.310	−0.738	0.047	15.5
3200	Phaethon	1983 TB	APO	B	B	−0.442	0.238	−0.010	14.6
8201		1994 AH2	APO		O	−0.199	−0.248	0.020	16.3
9969	Braille	1992 KD	MC		Q	0.086	−0.294	−0.090	15.8
10302		1989 ML	AMO		X	0.137	0.248	0.044	19.5
16064		1999 RH27	AMO		C	0.120	0.254	0.004	16.8
16834		1997 WU22	APO		S	0.548	−0.085	−0.019	15.2
18882		1999 YN4	AMO		S	0.303	−0.171	0.016	15.6
20043		1993 EM	MC		U	−0.101	0.058	0.058	15.4
		1996 FG3	APO		C	−0.079	0.250	−0.012	18.4
		1998 BG9	AMO		S	0.336	−0.153	0.029	19.5
		1998 BB10	APO		Sq	0.132	−0.143	0.081	20.5
		1998 BM10	MC		Sq	0.260	−0.122	0.050	16.5
		1998 BT13	APO		Sq	0.127	−0.170	0.059	26.5
		1998 MW5	APO		Sq	0.069	−0.366	−0.054	19.2
		1998 ST49	APO		Q	−0.090	−0.283	0.106	17.7
		1998 UT18	APO		C	−0.096	0.172	−0.008	19.0
		1998 WP5	AMO		Sl	0.772	−0.203	0.039	18.7
		1999 CF9	APO		Q	−0.134	−0.132	0.081	17.9
		1999 DJ4	APO		Sq	0.112	−0.209	−0.016	18.2
		1999 GJ4	APO		Sq	0.008	−0.257	0.100	15.1
		1999 JE1	APO		Sq	−0.083	−0.227	0.066	19.5
		1999 JU3	APO		Cg	0.044	0.100	−0.111	19.2
		1999 JV3	APO		S	0.574	−0.269	−0.050	19.0
		1999 JD6	ATE		K	0.503	0.022	−0.158	16.7
		1999 JV6	APO		Xk	0.280	0.055	−0.178	19.7
		1999 JO8	AMO		S	0.328	−0.269	−0.002	17.0
		1999 ND43	AMO		Sl	0.654	−0.157	0.099	19.1
		1999 RB32	AMO		V	−0.057	−0.577	−0.056	19.8
		1999 SE10	AMO		X	0.514	0.274	−0.038	20.0
		1999 SK10	APO		Sq	0.147	−0.163	−0.046	19.3
		1999 TX16	AMO		Ld	0.930	−0.063	0.037	15.7
		1999 VQ5	MC		Q	−0.100	−0.232	−0.025	19.4
		1999 VN6	AMO		C	0.057	0.243	0.027	19.5
		1999 VM40	AMO		S	0.570	−0.154	−0.014	14.4
		1999 WK13	AMO		S	0.430	−0.147	0.008	17.2
		1999 XO35	AMO		Sq	0.176	−0.204	−0.020	16.8
		1999 YB	AMO		Sq	0.273	−0.209	−0.101	18.2
		1999 YD	AMO		Sk	0.290	−0.123	−0.139	21.1
		1999 YF3	AMO		Sq	0.250	−0.097	−0.047	18.2
		1999 YG3	APO		S	0.526	−0.111	0.032	19.0
		1999 YK5	ATE		X	0.105	0.275	0.073	16.8
		2000 AC6	ATE		Q	−0.092	−0.175	−0.014	21.0
		2000 AX93	AMO		Sq	0.149	−0.155	0.010	17.4
		2000 AE205	AMO		S	0.534	−0.187	−0.071	22.9
		2000 AH205	APO		Sk	0.328	−0.212	−0.168	22.4

"S." Overall, the Bus (1999) results reveal that asteroids show a full continuum of spectral properties spanning the range within and between the boundaries of previously recognized groups. The Bus system utilizes a single or multiple letter designation such that objects intermediate between the "S" and "Q" classes, for example, have the designation "Sq."

Within Table I, the fourth column indicates the Apollo, Amor, Aten orbit class for each object. Three observed objects are currently categorized as "Mars crossers" (MC). The table includes a previously given taxonomic designation (if any is available) for each object followed by the designation in the Bus (1999) system. The key analysis parameters that feed into the Bus system are also tabulated—measures of the fitted spectral slope and the second and third components in a principal component analysis. (These components are labeled PC2′ and PC3′ so as not to be confused with principal component scores from previous work such as Tholen 1984.) The remaining column tabulates the H magnitude for each object.

A small number of main-belt asteroids were observed during the course of our Palomar NEO program. These data were generally obtained for the purpose of checking our overall calibration. For completeness, we present these results in Table II and Appendix B. Two additional Palomar-observed objects are described in separate publications. The outer main-belt object 1459 Magnya displays a V-type spectrum and is described by Lazzaro *et al.* (2000). The unusual class "Xe" spectrum of 64 Angelina is described by Burbine, Binzel, and Bus (in preparation).

(9969) Braille

Asteroid (9969) Braille (preliminary designation 1992 KD) was selected as an encounter target for the Deep Space 1 (DS-1) technology demonstration spacecraft, where the encounter occurred in July 1999 (Lehman 1999). Technically, Braille's perihelion distance is greater than 1.3 AU and it is not strictly categorized as a near-Earth object, but it is a Mars crosser. Our March and May 1999 Palomar observations of Braille revealed a deep 1-μm absorption band indicative of a silicate (pyroxene and/or olivine) composition. The spectrum is shown in Fig. 3. With visible wavelength data, it is difficult to make a conclusive distinction between the different silicate mineralogies. As a first step toward our analysis, we fit a spline through the reduced spectrum following the procedures outlined in Bus (1999). We next compared the original data and this spline fit to the two most likely meteorite analogs having deep 1-μm absorption bands: ordinary chondrites and eucrites. Figure 3a shows that we find the laboratory measurements for an ordinary chondrite to be virtually indistinguishable from the spline fit, while a eucrite spectrum shows a much steeper onset of the 1-μm absorption band beginning at a shorter wavelength than what our data reveal.

We also find that the spectral match (Fig. 3b) and the principal component scores for Braille (based on the spline fit) are virtually identical to those for 1862 Apollo, an object designated as taxonomic class "Q" and long considered an ordinary chondrite analog (McFadden *et al.* 1985). (Similar to the comparison with eucrite meteorites, we also see a poor fit to the V-type asteroid Vesta.) Based on the interpretation of our visible wavelength spectra we conclude that an ordinary chondrite-like composition and a Q taxonomic designation are the best determinations for this object. Properly and independently calibrated spectral data extending out into the near-infrared, as can easily be obtained with large aperture ground-based telescopes, can quickly confirm or refute this interpretation. Such broad wavelength coverage was also obtained by DS-1 (Soderblom *et al.* 1999).

(10302) 1989 ML

Asteroid (10302) 1989 ML had been selected as the primary target for the MUSES-C mission, but launch delays have shifted

TABLE II
Observational Results for Main-Belt Asteroids

Number	Name	Previous type	New type	Slope	PC2′	PC3′	H Magnitude
10	Hygiea	C	C	−0.055	0.287	−0.011	5.4
64	Angelina	E	Xe	0.433	0.223	0.061	7.7
143	Adria	C	C	0.125	0.267	−0.018	9.1
144	Vibilia	C	Ch	−0.180	0.390	−0.062	7.9
145	Adeona	C	Ch	0.029	0.381	−0.037	8.1
190	Ismene	X	C	0.067	0.312	0.021	7.6
336	Lacadiera	D	X	0.420	0.283	0.033	9.8
349	Dembowska	R	R	0.173	−0.471	0.008	5.9
375	Ursula	C	C	0.107	0.298	0.007	7.5
471	Papagena	S	Sk	0.251	−0.032	0.015	6.7
481	Emita	C	Ch	−0.092	0.364	−0.037	8.6
599	Luisa	S	T	0.778	0.133	−0.026	8.7
3628	Boznemcova	O	O	−0.379	−0.357	0.107	12.6
4552	Nabelek		S	0.593	−0.074	0.011	13.7
	1999 XH1		S	0.380	−0.319	−0.061	12.4

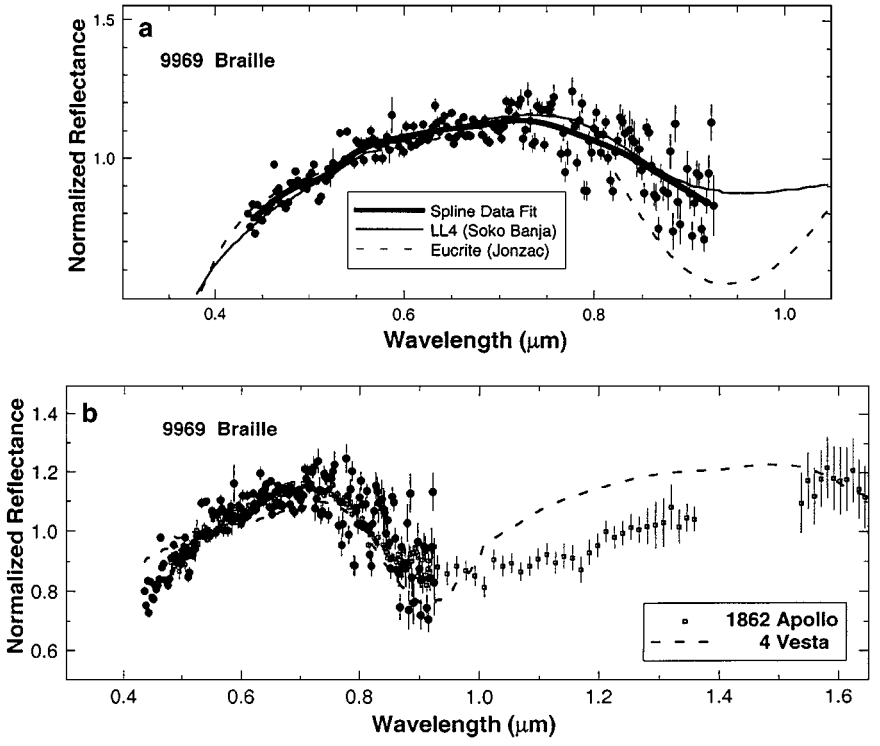

FIG. 3. (a, top) The Palomar spectrum of DS-1 spacecraft target (9969) Braille and the spline fit to these data. The LL4 ordinary chondrite meteorite (Soko Banja) provides a nearly indistinguishable match to the spline fit. The spectrum of a eucrite meteorite (Jonzac) shows a steeper slope at the onset of the absorption band and has a deeper band depth than what the data suggest. (b, bottom) The visual wavelength spectrum of (9969) Braille is fully consistent with that of (1862) Apollo but is a poor fit to the eucrite-like spectrum of (4) Vesta. Apollo is designated as a Q-type asteroid and is a previously suggested analog to ordinary chondrite meteorites. Meteorite data presented are from Gaffey (1976).

the mission destination to a different object. Nevertheless, 1989 ML remains one of the most attractive destinations for such missions because of the low propulsion requirements to reach it and return to Earth. Our Palomar observations of 1989 ML were obtained in March and May 1999 and the resulting spectrum is shown in Fig. 4. 1989 ML displays a relatively flat (neutral) spectrum that precludes a definitive compositional interpretation. Figure 4 presents a range of viable interpretations for analog meteorite types, and the best fit appears to be that of a black chondrite—an ordinary chondrite meteorite that has been darkened by the shock associated with an impact.

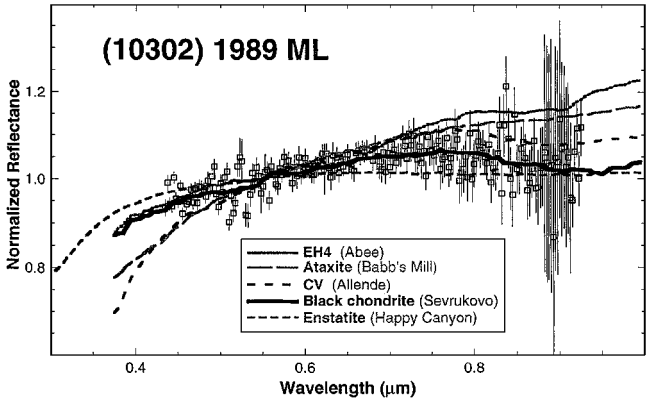

FIG. 4. Palomar spectrum for (10302) 1989 ML in comparison with five meteorite types that are viable matches to the neutral spectrum. The figure key denotes the meteorite analogs in the same order from top to bottom as they intersect the ordinate on the right side. A black chondrite (shock-darkened ordinary chondrite from Gaffey 1976) shows the best overall match to 1989 ML.

DISCUSSION

Our science goals extend greatly beyond the assignment of taxonomic designations to the measured objects. Here we discuss science results for the data set as a whole and for select groupings.

The S-Type to Q-Type Transition: The Connection to Ordinary Chondrite Meteorites

For many years 1862 Apollo (McFadden *et al.* 1985) existed as the only object residing in the Q-class, a class of objects having spectra similar to the most common meteorites, ordinary chondrites. The spectral differences between S- and Q-class objects (redder slopes and shallower absorption bands for the S-class) created a discontinuity between the spectral properties of the most common asteroids and the most common meteorites.

Figure 5 shows that spectral measurements of NEOs have eliminated this discontinuity by “filling the gap” between the

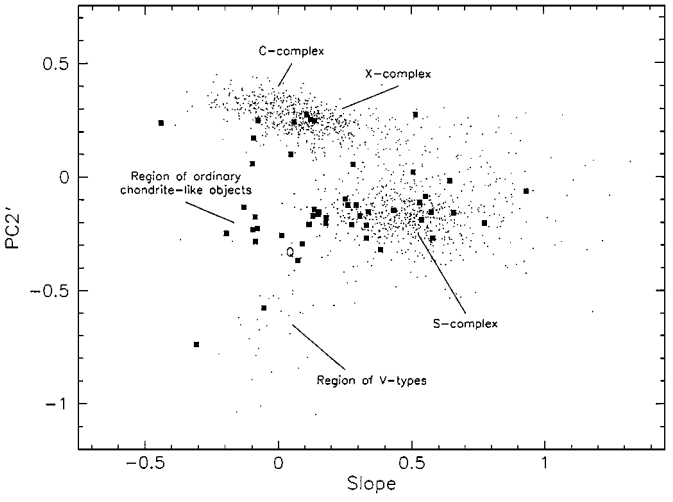

FIG. 5. Comparison of the spectral distribution between NEOs and main-belt asteroids. The analysis space consisting of the second principle component (PC2′) versus slope is derived from the work of Bus (1999). Main-belt objects are shown as small dots while the solid squares depict the observed NEOs. The substantially smaller data set on NEOs spans the full range for main-belt asteroids, and most notably, fills the gap between the S-asteroids (called the "S-complex") and ordinary chondrites. The previously unique ordinary chondrite-like asteroid 1862 Apollo has its location labeled "Q" denoting the region for this taxonomic type that is now populated by a significant sample of NEOs.

domains of the S and Q classes. This S- to Q-class transition within the NEO population was shown by Binzel *et al.* (1996) based on spectral properties measured over visible wavelengths. Figure 6 reaffirms this transition with the extension of the spectral coverage to near-infrared wavelengths. While these data show evidence for a connection between the most common asteroids and the most common meteorites, they do not reveal the nature of this connection. The transition of spectral properties between the S and Q classes appears to be continuous and suggests a continuous process that could be related to surface age and/or surface gravity (such as the ability to establish a regolith). While there is a long history of debate and uncertainty over whether such a process might exist and what it might be (e.g., Wetherill and Chapman 1988), recent work on the coating of grains by nanophase iron (Pieters *et al.* 2000) appears to provide a viable process.

About one-third (18 out of 48) of the objects in our sample have spectral properties that place them within the Sq and Q classes. These objects are therefore among those known to have the best spectral matches with ordinary chondrite meteorites. Combined visible and near-IR measurements are available for eight of these and Fig. 7 compares their spectra directly with laboratory measurements of ordinary chondrite meteorites.

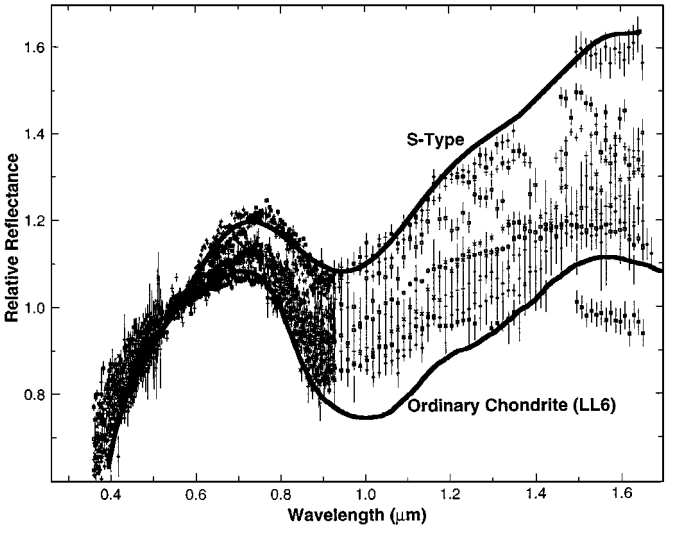

FIG. 6. A continuous transition in visible and near-infrared spectral properties is seen between the solid lines depicting typical S-type asteroids and ordinary chondrite meteorites. All S-, Sq-, and Q-type NEOs having both Palomar and IRTF data are depicted as points. The meteorite spectrum is an average for LL6 ordinary chondrites from Gaffey (1976).

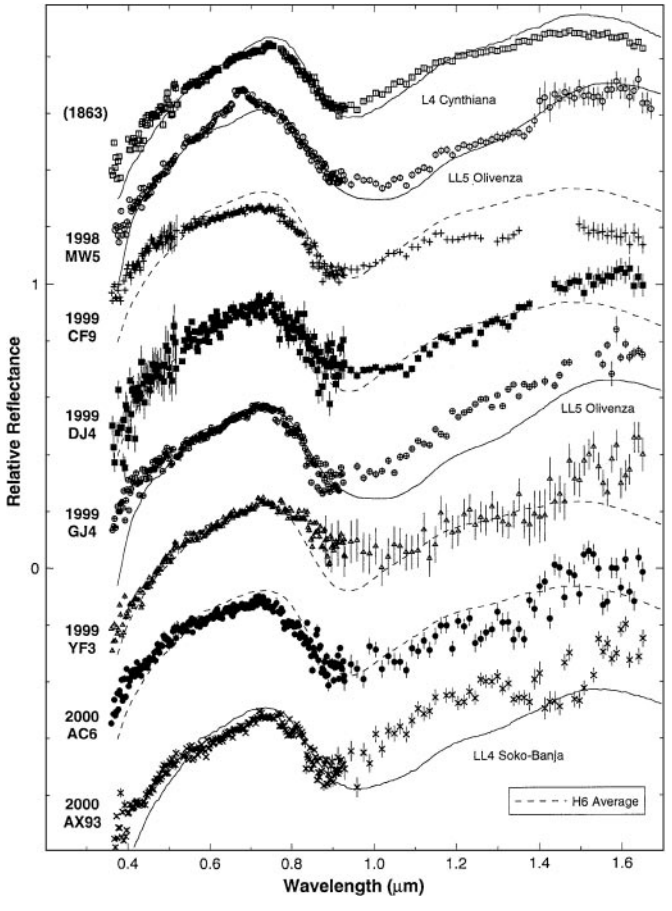

FIG. 7. Sq- and Q-type asteroids having full wavelength coverage generally show reasonable fits to laboratory measurements of ordinary chondrite meteorites (Gaffey 1976). Potential ordinary chondrite meteorite sources may not be rare within the near-Earth object population.

Diversity of NEO Spectral Types and Unusual Objects

One of our principal science goals is to understand the distribution of NEO spectral properties, particularly as they compare with larger main-belt asteroids. One important trend regarding the spectral diversity of NEOs is revealed by these Palomar and IRTF data. Figure 5 shows the principal component space (Bus 1999) for these near-Earth objects and reveals that NEOs display a much broader spectral diversity than is seen for main-belt asteroids. While many NEOs fall within the regions defining the loci for classical C-type and S-type asteroids (referred to as "complexes" by Bus 1999), the much smaller sample population of NEOs spans the whole range of slope within both the C and S complexes. Most notable is the filling of the region between the S asteroids and class Q and the abundance of Q-class objects, as discussed above.

Spectra for unusual objects in other classes are shown in Fig. 8, where each is compared with a meteorite type. Objects falling within the K class are most abundantly located within the Eos family in the outer region of the main belt. Their spectra have been noted to resemble CO/CV chondrites (e.g., Bell 1988, Doressoundiram *et al.* 1998, Burbine *et al.* 2001), but objects in this class have been rare or absent within near-Earth space. Our observations of 1999 JD6 place this NEO in the K class and Fig. 8 shows its very close match to CV meteorites. Asteroid 8201 displays a very unusual visible spectrum placing it in the O-class, previously occupied only by main-belt asteroid 3628 Boznemcova (Binzel *et al.* 1993). The blue channel of the Palomar spectrograph and the IRTF extension into the near-infrared spectrum of 3628 Boznemcova allow a more critical look at the potential meteorite analog for these O-class asteroids. While Binzel *et al.* (1993) made a case for a resemblance to ordinary chondrite meteorites, comparison with the same meteorite over the broader spectral range shows that this resemblance does not hold up. The mismatch at the short-wavelength end (noted by Chapman 1996) is considerably pronounced with the new data. On the long-wavelength end, Boznemcova displays a very unusual symmetric bowl-shaped 1-μm feature. If this feature is due to some type of pyroxene, it is a pyroxene type that is not abundant in measured meteorite samples. Burbine (2000) noted that augite (a calcic clinopyroxene found in some ureilites) has a broad symmetric bowl-like absorption feature, but this mineral feature is much wider than observed in either 3628 or 8201. Finally, we note two V-class objects within our NEO sample—1981 Midas and 1999 RB32—which display good spectral matches to eucrite meteorites. Their spectra are also similar to Vesta and the "Vestoids" (Binzel and Xu 1993) and may be related.

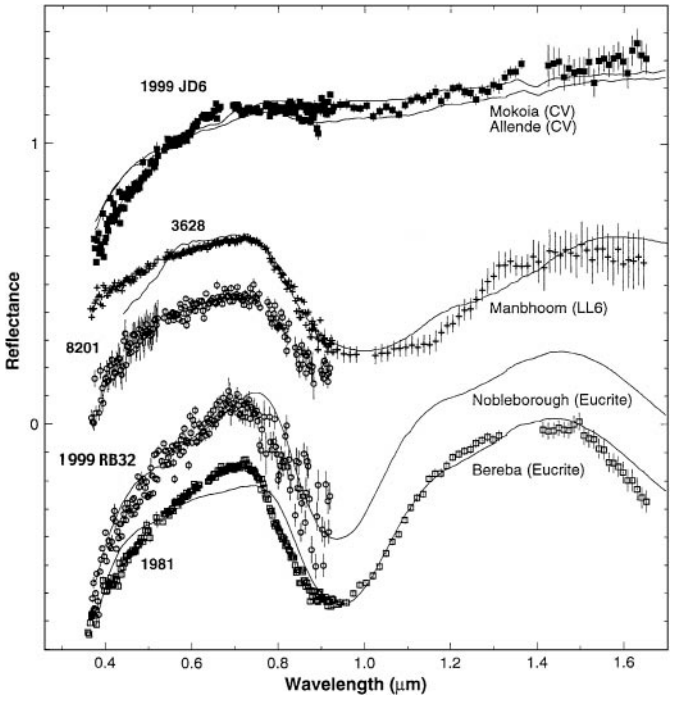

FIG. 8. Objects having particularly unusual spectral characteristics (data points) are shown in comparison with potential meteorite analogs (lines). 1999 JD6 falls within the K class and shows an excellent fit to primitive CV chondrites. Near-Earth object 8201 resembles the unusual O-class object 3628 Boznemcova. The extended spectral coverage for Boznemcova now available shows sufficient mismatch to ordinary chondrite meteorites to refute the meteorite resemblance proposed by Binzel *et al.* (1993). Both 1981 Midas and 1999 RB32 fall in the V class and show good matches to eucrite meteorites. All spectra are offset vertically for clarity. Meteorite spectra are from Gaffey (1976).

CONCLUSIONS

Because of their proximity, near-Earth objects are the smallest solar system bodies that can be telescopically measured. Their proximity also makes them the closest analogs (and likely the immediate sources) for meteorites. While ordinary chondrite-like asteroids have been rare or absent in the main belt, we find them to be relatively common within the near-Earth population. The continuous transition we find between the spectral properties of S-asteroids and ordinary chondrite meteorites provides direct evidence for the occurrence of a continuous natural process such as space weathering. The ordinary chondrite end members of this transition could simply be the ones with the youngest and freshest surfaces. We can expect near-Earth asteroids to have surfaces displaying a wide range of ages, most especially younger ages, since collisions that generate new objects or fresh surfaces become much more frequent at small sizes.

The greater overall diversity of spectral properties seen within the NEO population of small objects could also be a consequence of space weathering where we are seeing a broad range from older to younger surfaces. The diversity at small sizes could also arise if these objects tend to sample monomineralogic units from once larger parent bodies. If these distinct units are present on larger asteroids, they are not so clearly revealed since Earth-based spectral measurements sample the average reflectance of an entire hemisphere.

APPENDIX A: SPECTRA FOR NEAR-EARTH OBJECTS

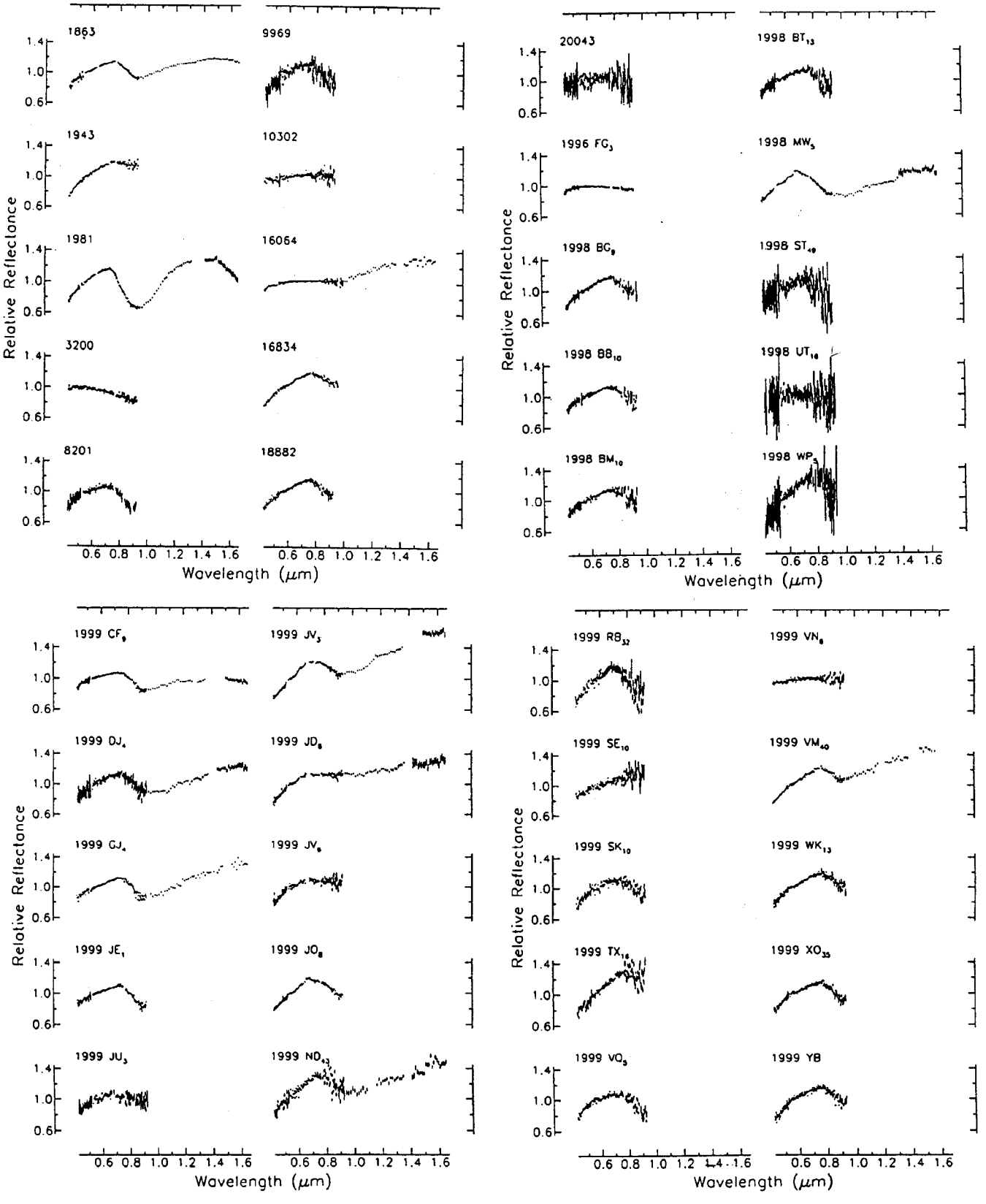

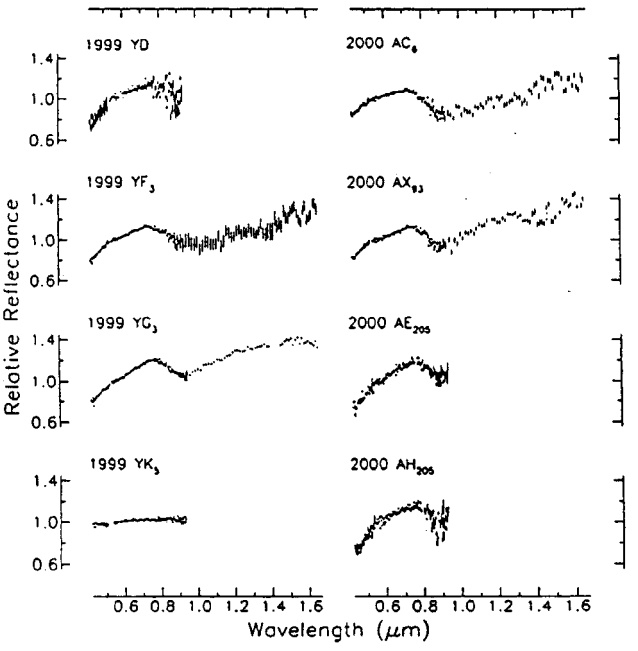

APPENDIX B: SPECTRA FOR MAIN-BELT OBJECTS

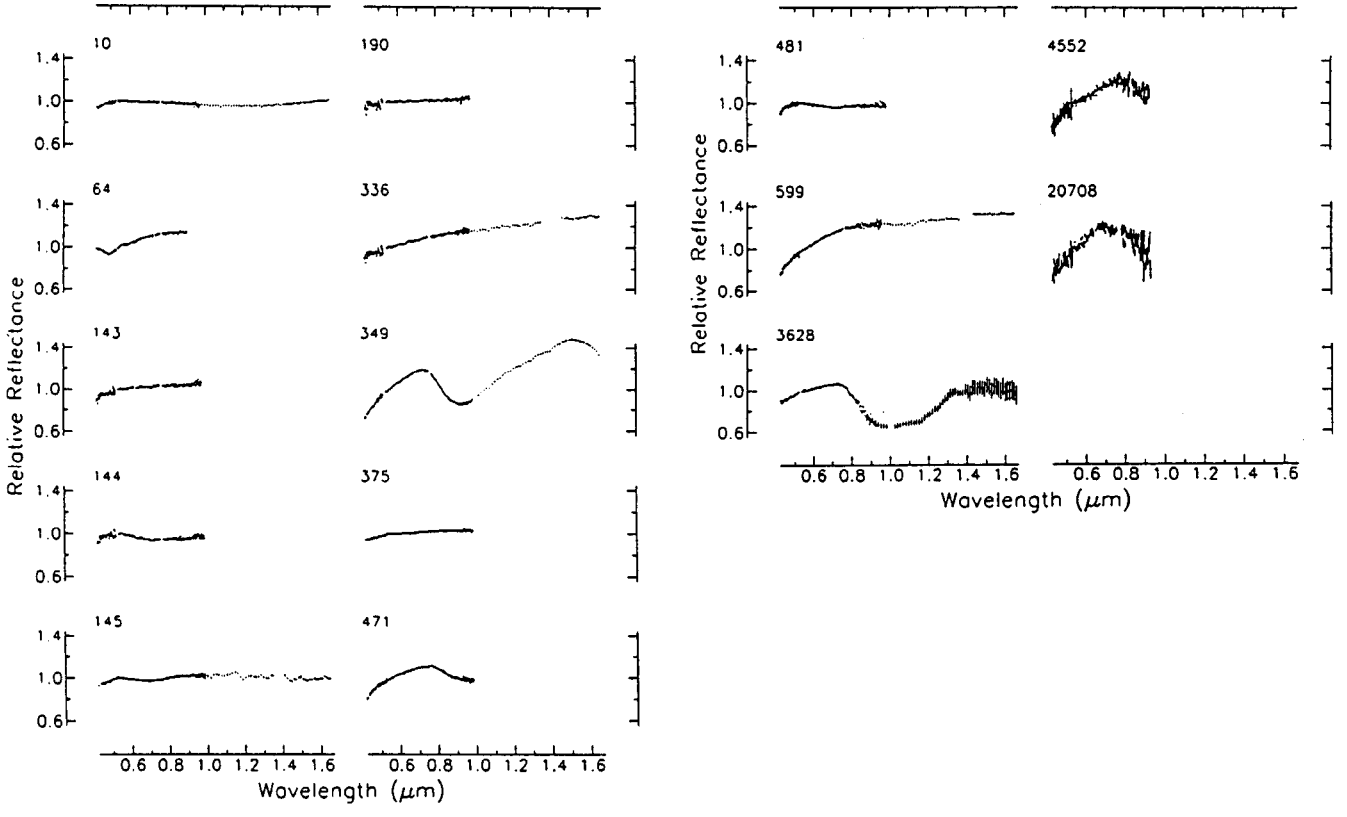

ACKNOWLEDGMENTS

Results in this paper are based on observations obtained at the Hale Telescope, Palomar Observatory as part of a continuing collaboration between the California Institute of Technology, NASA/JPL, and Cornell University. The authors also acknowledge their being Guest Observers at the Infrared Telescope Facility, operated by the University of Hawai'i under contract to the National Aeronautics and Space Administration. We thank April Deet for dedicated assistance with the IRTF data processing. This work was supported by NASA Grant NAG5-3939 and NSF Grant AST-9530282. The work at the Jet Propulsion Laboratory, Caltech, was supported under contract from NASA.

REFERENCES

Bell, J. F. 1988. A probable asteroidal parent body for the CV or CO chondrites. *Meteoritics* **23**, 256–257.

Binzel, R. P., and S. Xu. 1993. Chips off of Asteroid 4 Vesta: Evidence for the parent body of basaltic achondrite meteorites. *Science* **260**, 186–191.

Binzel, R. P., S. Xu, S. J. Bus, M. F. Skrutskie, M. Meyer, P. Knezek, and E. S. Barker, 1993. Discovery of a main-belt asteroid resembling ordinary chondrite meteorites. *Science* **262**, 1541–1543.

Binzel, R. P., S. J. Bus, T. H. Burbine, and J. M. Sunshine 1996. Spectral properties of near-earth asteroids: Evidence for sources of ordinary chondrite meteorites. *Science* **273**, 946–948.

Burbine, T. H. 2000. *Forging Asteroid-Meteorite Relationships Through Reflectance Spectroscopy*. Ph.D. thesis, Massachusetts Institute of Technology, Cambridge, MA.

Burbine T. H., R. P. Binzel, S. J. Bus, and B. E. Clark 2001. K asteroids and CO3/CV3 chondrites. *Meteoritics Planet. Sci.* **36**, 245–253.

Bus, S. J. 1999. *Compositional Structure in the Asteroid Belt.* Ph.D. thesis, Massachusetts Institute of Technology, Cambridge, MA.

Chapman, C. R. 1996. S-type asteroids, ordinary chondrites, and space weathering: The evidence from Galileo's fly-bys of Gaspra and Ida. *Meteoritics Planet. Sci.* **31**, 699–725.

Doressoundiram, A., M. A. Barucci, M. Fulchignoni, and M. Florczak 1998. Eos family: A spectroscopic study. *Icarus* **131**, 15–31.

Gaffey, M. J. 1976. Spectral reflectance characteristics of the meteorite classes. *J. Geophys. Res.* **81**, 905–920.

Lazzaro, D., T. Michtchenko, J. M. Carvano, R. P. Binzel, T. H. Burbine, T. Mothe-Diniz, M. Florczak, C. A. Angeli, and A. W. Harris 2000. *Science* **288**, 2033–2035.

Lehman, D. H. 1999. Deep Space 1 mission overviews. *Bull. Am. Astron. Soc.* **31**, 1127.

McFadden, L. A., M. J. Gaffey, and T. B. McCord, 1985. Near-Earth asteroids: Possible sources from reflectance spectroscopy. *Science* **229**, 160–163.

Oke, J. B., and J. E. Gunn 1982. An efficient low resolution and moderate resolution spectrograph for the Hale Telescope. *Publ. Astron. Soc. Pacific* **94**, 586–594.

Pieters, C. M., L. A. Taylor, S. K. Noble, L. P. Keller, B. Hapke, R. V. Morris, C. C. Allen, D. S. McKay, and S. Wentworth 2000. Space weathering on airless bodies. *Meteoritics Planet. Sci.* **35**, 1101–1108.

Soderblom, L., D. Boice, D. Britt, R. Brown, B. Buratti, J. Hicks, M. Hillier, R. Lee, R. Meier, J. Nelson, T. Oberst, A. Owen, A. Rivken, A. Sandel, N. Stern, R. Thomas, R. Yelle 1999. Deep Space 1 MICAS observations of 9969 Braille. *Bull. Am. Astron. Soc.* **31**, 1127.

Tholen, D. J. 1984. *Asteroid Taxonomy from Cluster Analysis of Photometry*. Ph.D. thesis, University of Arizona, Tucson.

Tholen, D. J. 1989. Asteroid taxonomic classifications. In *Asteroids II* (R. P. Binzel, T. Gehrels, and M. S. Matthews, Eds.), pp. 1139–1150. Univ. of Arizona Press, Tucson.

Wetherill, G. W., and C. R. Chapman (1988). Asteroids and meteorites. In *Meteorites and the Early Solar System* (J. F. Kerridge and M. S. Matthews, Eds.) pp. 35–67. Univ. of Arizona Press, Tucson.

Xu, S., R. P. Binzel, T. H. Burbine, and S. J. Bus 1995. Small main-belt asteroid spectroscopic survey: Initial results. *Icarus* **115**, 1–35.